

# Local tetragonal distortion in $La_{0.7}Sr_{0.3}MnO_3$ strained thin films probed by x-ray absorption spectroscopy

Narcizo M. Souza-Neto,\* Aline Y. Ramos,† and Hélio C. N. Tolentino

Laboratório Nacional de Luz Síncrotron - LNLS, P.O. Box 6192, 13084-971, Campinas, São Paulo, Brazil

Emmanuel Favre-Nicolin and Laurent Ranno

Laboratoire Louis Néel, UPR 5051 CNRS-UJF, Grenoble, France

(Dated: 23rd September 2018)

We report on an angular resolved X-ray Absorption Spectroscopy study of  $La_{0.7}Sr_{0.3}MnO_3$  thin films epitaxially grown by pulsed laser deposition on slightly mismatched substrates which induce tensile or compressive strains. XANES spectra give evidence of tetragonal distortion within the  $MnO_6$  octahedra, with opposite directions for tensile and compressive strains. Quantitative analysis has been done and a model of tetragonal distortion reflecting the strain has been established. EXAFS data collected in plane for tensile substrate confirm the change in the  $Mn-O$  average bond distance and the increase of  $Mn-Mn$  length matching with the enlargement of the cell parameter. From these results we conclude that there is no significant change in the  $Mn-O-Mn$  angle. Our observations conflict with the scenarios which this angle is the main driving parameter in the sensitivity of manganite films properties to external strains and suggest that the distortion within the octahedra plays a key role in the modification of the transport and magnetic properties.

PACS numbers: 75.47.Lx, 68.55.-a, 78.70.Dm, 33.15.Dj, 31.15.Ar

## I. INTRODUCTION

The delicate balance between orbital and spin interactions in doped manganites ( $RE_{1-x}A_xMnO_3$ ,  $RE$  = rare earth, and  $A$  = alkaline metal) leads to many interesting exotic properties. Among them the colossal magneto-resistance brought about the stir of interest for this class of material<sup>1,2,3</sup>. It has been largely reported that the remarkable properties of doped manganites show drastic sensitivity to small changes in their structural parameters and the form of the samples<sup>4,5</sup>. At the atomic level this versatility is correlated to distortion within the manganese coordination octahedra  $MnO_6$  and modifications in the angle  $\varphi = Mn-O-Mn$ <sup>1,6,7</sup>. The  $Mn^{3+}$  ion has an high-spin  $t_{2g}^3 e_g^1$  configuration and the deformation of the metal-ligand octahedra stems from the Jahn-Teller interaction, that tends to lift the degeneracy of the  $d$  orbitals and stabilize the energy levels of the occupied  $d$  electron. The angle  $\varphi$  is  $\pi$  in a cubic structure, but is bent and deviated from  $\pi$  in non-cubic compounds. Thin films of manganites, grown using deposition techniques similar to the ones developed for high-temperature superconductors (pulsed laser deposition, sputtering, MOCVD, ...), drawn large possibilities in the design of tunable magnetic devices<sup>8</sup>. Thus it has been early observed that manganites films display properties significantly different from those of the bulk material and these properties are dependent on the film thickness<sup>4,8,9,10</sup>. One prominent example is the decrease of the Curie temperature  $T_C$  as the strain increases<sup>11,12</sup>. This characteristic has been associated to the strain induced by the lattice mismatch. It should be noted that in bulk manganites the sensitivity of  $T_C$  for applied hydrostatic pressure and "chemical" pressure, i.e. structural distortion changing the average radius of the atom in the  $A$  site, is well known and associated to modification in angle  $\varphi$ . This correlation is simply derived when one remembers that description of the transport and magnetic properties are determined by the effective intersite hopping

$t_{ij}$  of the  $e_g$  electrons via O  $2p$  states that controls the double exchange. In the strong ligand field approximation the  $p-d$  transfer interaction is scaled as  $t_{pd} = t_{pd}^\circ \cos(\varphi)$ , ( $t_{pd}^\circ$  transfer interaction for  $\varphi = \pi$ ) then  $T_C$  is almost proportional to  $\cos^2 \varphi$ <sup>6,7,13</sup>. As  $t_{pd}^\circ$  depends on the  $Mn-O$  distance, the transport properties are also expected to vary with this distance. To understand the correlation between the substrate-induced strain and the modifications of the transport and magnetic properties in thin films, it is then important to explicit the connection between the crystallographic cell strains and the modifications in the local parameters<sup>6,9,14</sup>. Several experimental studies by X-ray Absorption spectroscopy have addressed the local organization in manganites films, and variations of the local environment in thin films versus bulk samples, pointing out the importance of the local distortion around  $Mn$ <sup>15,16,17</sup>. At the moment it does not seem that a full consensus is reached about what the main distortion at the local scale is. In  $La_xCa_{1-x}MnO_3$  films, with  $x$  close to 0.7, Miniotas and coworkers<sup>16</sup> do not observe any modification within the coordination shell, but reported on variations of the Mn-Mn distance, according to the substrate misfit strain. They conclude that the biaxial strain is accommodated by appropriate bending of the  $Mn-O-Mn$  angle. On the other hand thickness-dependent  $Mn$  coordination asymmetry is reported in thin film of the system  $Nd_{0.5}Sr_{0.5}MnO_3$  close to the charge-ordered state<sup>17</sup>. These results suggest the importance of the biaxial strain on the electron localization, quite different from the effect of an hydrostatic pressure.

$La_{0.7}Sr_{0.3}MnO_3$  manganite exhibits ferromagnetic transition around room temperature ( $T_c \approx 360K$ <sup>4,5,7,18</sup>) and fully spin-polarized conduction band. These characteristics made this compound attractive as low cost magnetic sensor and a perfect model material for correlated electrons properties.  $La_{0.7}Sr_{0.3}MnO_3$  crystallize in a the rhomboedral  $R\bar{3}c$  ( $D_{3d}^6$ ) variant of the cubic perovskite, with  $La$  and  $Sr$  randomly distributed on the  $A$  site (6a positions)<sup>5,13</sup>. The ratio be-

tween the cell parameter  $a$  and  $c$  is close to  $1/\sqrt{2}\sqrt{3}$ , so that this structure can be considered as “pseudo-cubic” with  $a=3.87\text{\AA}$ . From the crystallographic data the angles  $\varphi$  are close to  $165^\circ$  and there is no distortion of the  $MnO_6$  octahedra. A measure of this distortion is given as the root square deviation of the  $Mn-O$  distances from their average value:  $\sigma_{JT} = \sqrt{\frac{1}{3}\sum_i [(Mn-O)_i - \langle Mn-O \rangle]^2}$ , which is of about  $1.2 \times 10^{-1}\text{\AA}$  in the prototype Jahn-Teller compound  $LaMnO_3$  at room temperature associated to the strong localization of the  $e_g$  electron. In the metallic  $La_{0.7}Sr_{0.3}MnO_3$  compound, the  $e_g$  electron is delocalized and the contribution of the spontaneous energy-lowering Jahn-Teller distortion of the  $Mn^{3+}O_6$ <sup>18,19</sup> does not give rise to a measurable average distortion of the octahedra. In X-ray absorption spectroscopy (XAS) the coordination shell around Mn atoms can be modelled with one unique  $Mn-O$  distance at  $\approx 1.94\text{\AA}$ <sup>20,21</sup>.

In a precedent paper<sup>22</sup> we reported on the evidence of distortion within the coordination octahedra around the Mn in  $La_{0.7}Sr_{0.3}MnO_3$  thin films from the angular dependence of the XANES (X-ray Absorption Near Edge Structure) spectra in strained films. In the present paper this study has been completed by new set of data, a quantitative analysis of the XANES spectra using the Natoli’s rule<sup>23</sup> and of EXAFS (Extended X-ray Absorption Fine Structure) measurements in the plane of strained and relaxed films. This complete set of experimental results is combined to *ab initio* calculation of angular resolved XAS for a local distortion in tensile and compressive substrates, that account for the angular dependence of the spectra. We found a tetragonal distortion of the  $MnO_6$  and no significant modifications in the  $Mn-O-Mn$  angle. These findings stress the importance of the distortion of the ligand field around the manganese atoms. The strain-induced modification in the film properties should then be mainly ascribed to  $t_{pd}^0$  and the variations of hybridization between the metal and ligand orbitals, which tends to localize the  $e_g$  electron at the  $Mn$  site. In the section II we present the basis of the angular resolved X-ray Absorption Spectroscopy and remind the basis of the Natoli’s rule and the principles of data analysis. In section III we give the characteristics of the sample and thoroughly describe the experiments. The results obtained from XANES and EXAFS analysis are detailed and discussed in section IV and V. The prominent aspects of this study are then summarized in section VI.

## II. X-RAY ABSORPTION SPECTROSCOPY

The absorption cross section  $\sigma(\omega)$ , ratio between the absorbed energy and the incident photon flux, is given by the summation over all possible final states of the transition probability from the initial  $|i\rangle$  to a final state  $|f\rangle$ . In the dipolar approximation of Fermi’s Golden Rule<sup>24</sup>, each probability can be expressed by  $|\langle f|\hat{\epsilon}\cdot\vec{r}|i\rangle|^2$ . Due to the dot product  $\hat{\epsilon}\cdot\vec{r}$ , the absorption cross section in anisotropic media has the same structure as the dielectric constant and can be described by a tensor of rank two, whose expression depends on the point group of the media<sup>24</sup>. If the studied system is

randomly oriented, the contribution of the dipole interaction to the absorption coefficient reflects an average of the contributions in all orientations. In oriented systems, the contribution of each dipole interaction term can be selected. The simplest expression of the dichroic effect is obtained for non-cubic samples, with a rotation axis of order greater than two, where one can find two different cross sections. For this particular case, and expressing in terms of the linear absorption coefficient  $\mu \propto \sigma(\omega)$ , one defines two parameters:  $\mu_{\parallel}$  stands for the absorption coefficient when the electric vector lies in a plane orthogonal to the rotation axis and  $\mu_{\perp}$  is the coefficient when the electric vector is along the rotation axis. For any given orientation of the electric vector, measured by the angle  $\theta$  related to that rotation axis,  $\mu(\theta)$  reads:

$$\mu(\theta) = \mu_{\parallel}\sin^2\theta + \mu_{\perp}\cos^2\theta \quad (1)$$

This expression is valid over the whole energy XAS range<sup>24</sup>. Selective pieces of information can be extracted using angle-resolved XAS, as long as oriented samples are available. Angle resolved XAS is widely used to improve the results of conventional analysis and enhances the sensitivity of XAS to probe very tiny difference in anisotropic systems, like anisotropic single-crystals<sup>25,26</sup>, surfaces<sup>27</sup> and multilayers<sup>28</sup>.

The angle resolved EXAFS data have been analyzed following standard procedures<sup>29</sup>. For the analysis of the XANES data we combined to *ab initio* simulations, a semi-empirical approach based on the so called Natoli’s rule<sup>23</sup>.

XANES  $Mn$  K-edge spectra were calculated by real space full multiple scattering using the Feff8.2 code<sup>30</sup>. The potentials are modeled with the Hedin-Lundqvist exchange correction, taking into account a single hole in  $Mn$  1s orbital, without screening effect. Atomic positions are given for a set of atoms whose centers are located at a distance  $R_c$ . The electric field vector polarization is defined in relation with the atomic structure orientation, and then all the photoelectron scattering terms, are weighted using the equation (1). This procedure enables to calculate independently the information from the different angular contributions to the absorption.

The calculations are conducted self consistently in a sphere of radius  $RSCF$ , providing a calculation of the Fermi energy ( $k=0$ ) accurate to a couple of eV. Full multiple scattering is taken into account for  $R_c < RFMS$ , while only single scattering contributions are contemplated for outer atoms. No specific dynamical contribution to the disorder (Einstein or Debye model) was introduced in the calculations. The radial disorder has been modeled by a Gaussian broadening, where  $\sigma$  has been approximated by the Debye-Waller factor obtained from the EXAFS analysis of the coordination shell ( $\sigma = 0.06\text{\AA}$ ). The broadening due of the experimental energy resolution has been partially taken into account by including a shift of 0.6eV in the imaginary part of the potential. The calculated spectra were normalized by the value at 50eV above the absorption edge and a small energy shift of -1.8 eV has been applied to fit the edge position in the experimental data.

The Natoli’s rule expresses the linear relationship between the wave vector of the photoelectron at a multiple scattering resonance, and  $1/R$ , where  $R$  is the distance to the nearest neighbors. It is justified theoretically within the framework

Table I: Samples nomenclature and characteristics obtained by X-ray diffraction. Biaxial strain factors can then be defined as  $\epsilon_{\parallel} = \frac{a_{\parallel} - a_{\text{bulk}}}{a_{\text{bulk}}}$  and  $\epsilon_{\perp} = \frac{a_{\perp} - a_{\text{bulk}}}{a_{\text{bulk}}}$ , where  $a_{\parallel}$  and  $a_{\perp}$  are the in plane and out of plane lattice parameters of films respectively.

Composition (nomenclature)	Strain (relaxation)	Thickness (relaxation)	Lattice parameter	Strain factors $\epsilon_{\parallel} (\epsilon_{\perp})$
$La_{0.7}Sr_{0.3}MnO_3$ (LSMO)	-	$\infty$	3.87Å	-
$LaAlO_3$ (LAO300)	Fully relaxed	300nm ( $t_c \approx 30nm$ )	3.793Å	$\approx 0\%$
$LaAlO_3$ (LAO45)	Compressive ( $\approx 10\%$ relaxed)	45nm ( $t_c \approx 30nm$ )	3.793Å	-2.0% (2.3%)
$MgO$ (MO60)	Fully relaxed	60nm	4.21Å	$\approx 0\%$
$SrTiO_3$ (STO60)	Tensile (fully strained)	60nm ( $t_c \approx 100nm$ )	3.905Å	0.9% (-0.8%)

of the multiple scattering theory. The absorption cross section is determined by the multiple scattering matrix  $M$  of the photoelectron with kinetic energy  $(\hbar k)^2/2m = E_r - E_0 + V$ , with  $E_r$  energy of the resonance,  $E_0$  absorption threshold and  $V$  average muffin-tin interstitial potential. The maxima of the absorption correspond to the condition  $DetM = 0$ , giving the relation  $k \cdot R = constant$ . The extraction of the variation of the interatomic distance in unknown systems is complicated by the determination of  $k = [\hbar/2m(E_r - E_0 + V)]^{1/2}$  because  $V$  is unknown and cannot be determined experimentally. To overcome this problem the energy separation of a multiple resonance in the continuum from a bound state at the threshold  $\Delta E_r = (E_r - E_b)$  can be used to determine the variation of the interatomic distance<sup>23</sup>. The rule is then expressed under its usual form :

$$(E_r - E_b)R^2 = K \quad (2)$$

This rule is valid only for a range of about 20% variation of the interatomic distance  $R$ , where the energy dependence of the scattering phase shifts is negligible. It has been successfully applied to the case of Cu-O bonds in a large series of high temperature superconductors<sup>25</sup>. In these systems the constant  $K$  was found to be about  $46eV \cdot \text{\AA}^2$ . This corresponds to a  $\Delta E_r = 11.4eV$  for a  $Cu - O$  bond of  $1.95\text{\AA}$ <sup>25</sup>.

### III. EXPERIMENTAL

The  $La_{0.7}Sr_{0.3}MnO_3$  (LSMO) thin films have been epitaxially grown in the [001] direction by pulsed laser deposition under tensile ( $SrTiO_3$  [001]) and compressive ( $LaAlO_3$  [001]) substrates with cubic and pseudo-cubic structures. The small lattice mismatch between LSMO, STO and LAO allows a pseudomorphic growth and the films are fully constrained for thickness below the critical thickness ( $t_c$ ) for each case<sup>11,31</sup>. MgO substrate (cubic) with large lattice mismatch (9%) was used to obtain an unstrained textured film. A summary of the sample characterization by X-ray diffraction is given in table I, and more details can be found elsewhere<sup>11,31</sup>.

The x-ray absorption experiments were performed at the D04B-XAS beamline of the Brazilian synchrotron light laboratory (Laboratório Nacional de Luz Síncrotron, LNLS) in Campinas<sup>32</sup>, Brazil at the Mn K-edge (6.5keV). The monochromator was a Si (111) channel-cut. An ion chamber monitored the incident beam. 0.5 mm-slits selected beam in the orbit plane ( $\Psi = 0$ ) with an acceptance of 0.03mrad.

The light on the sample was predicted to be more than 99% linearly polarized<sup>33</sup>. The XANES spectra were collected in the range 6440 to 6700eV with 0.3eV-energy steps. The instrumental energy resolution was 1eV, of the same order as the core hole width (1.16eV), leading to an overall resolution of 1.5eV. During a sequence of XANES experiments, thermal effects in the optics induce a small energy shift. This shift was carefully monitored by recurrent collections of the XANES spectra of a Mn metal foil (edge in 6539.1eV). The energy scale of the XANES spectra were then corrected using this calibration curve. Moreover the corrected energy scale was checked by performing the same operations on second set of XANES data collected in a inversed time sequence. Energy shifts as small as 0.1eV are certified. The XANES were normalized at about 150eV above the edge to be compared in intensity.

The experimental setup included a goniometer with the rotation axis perpendicular to the orbit plane. The sample plates with surface of  $5 \times 5mm^2$  were placed on the goniometer with the surface aligned with the goniometer axis. The spectra were collected in two geometries: with the electric field of the incident linearly polarized photon beam set approximately parallel ( $\mu_{\parallel}$ ) and perpendicular ( $\mu_{\perp}$ ) to the film surface. Actually the working angles were  $10^\circ$  and  $75^\circ$ , that can induce systematic errors for  $\mu_{\parallel}$  and  $\mu_{\perp}$ . But these errors are low ( $<3\%$  for  $\mu_{\parallel}$  and about 7% for  $\mu_{\perp}$ )(eq. (1)) and have been dismissed. For  $\mu_{\parallel}$  measurements the beam size at the sample holder was  $0.1 \times 4.5mm^2$ . The lateral size of the beam was reduced by a factor 4 for  $\mu_{\perp}$  measurements.

To check possible errors in the alignment, as well as any kind of sample anisotropy in the plane, the sample, with a given  $\theta$  were also mounted on a goniometer with rotation axis along the propagation axis of the photons beam.  $\mu_{\theta}$ -XANES spectra with the same  $\theta$  but rotated around the propagation axis beam were then collected. The spectra were identical according to the experimental error, confirming that the samples are isotropic in the plane

Data acquisition were performed in the fluorescence mode collecting the Mn  $K_{\alpha}$  (near 5.90keV) photons using a Ge 15-elements solid state detector. With this photons energy, about  $10\mu m$  of substrate is probed beyond the whole films (25 to 300nm). This raises no much trouble for  $STO$  substrate, but for  $LAO$  substrate, the  $La - L_{\alpha,\beta_1,\beta_2,\gamma}$  fluorescence lines of the substrate are more intense, and superimposed to the magnitude of the  $Mn - K_{\alpha}$  fluorescence and their contribution cannot be totally dumped by the selection window. In the  $LAO45$  sample, the total acquisition time reaches a minimum of 4 min

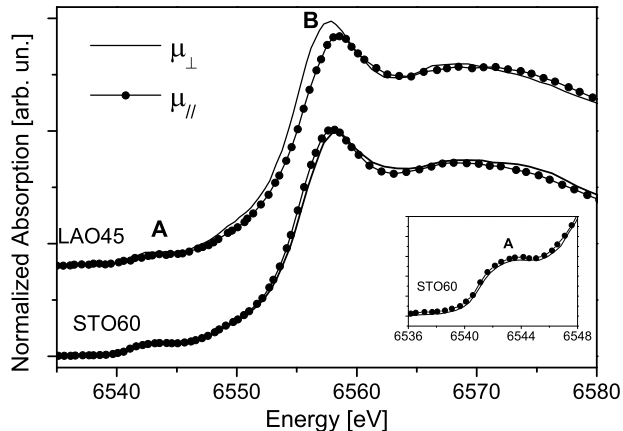


Figure 1: Experimental XANES spectra for the  $\mu_{\perp}$  and  $\mu_{\parallel}$  contributions in LAO45 and STO60 films. The Inset shows the pre-edge structure for STO60 film.

per point for the XANES range, and EXAFS data with satisfactory signal over noise ratio could not be collected. For the La-free substrates (STO and MO) due to the reduced beam size and the occurrence of a large number of Bragg peaks in this geometry, it was not possible to obtain  $\mu_{\perp}$  EXAFS data of the required quality. Only  $\mu_{\parallel}$  EXAFS data were collected, over 800eV above the edge.

## IV. RESULTS

### A. Mn-K XANES

The  $\mu_{\parallel}$  and  $\mu_{\perp}$  XANES spectra for tensile and compressive films (fig. 1) show the classical features observed in manganese compounds<sup>17,34</sup>: pre-edge peaks (A)<sup>35,36</sup>, arising from p-d mixing transition when the  $O_h$  symmetry is broken and relatively sharp rising edge and broad band resonances, dominated by the "white line" (labelled resonance B) assigned to transitions to  $4p$  empty states.

In the pre-edge range no difference can be evidenced between the angle resolved  $\mu_{\parallel}$  and  $\mu_{\perp}$  (fig. 1, insert), or between of the angle resolved XANES of the strained films and the isotropic spectra of the relaxed ones.

Above the rising edge two main effects are observed: an energy shift in the position of the main jump and correlatively in that of the resonance B, and changes in the shape and amplitude of this resonance. The shifts for the tensile and compressive films are in opposite directions. For the tensile substrate STO60, the negative energy shift (-0.4eV) in the in-plane spectrum shows that the average  $Mn-O$  bond length is larger in the film plane than out-of-plane of the film. On the other hand in the film LAO45 under compressive strain, the positive energy shift (+0.9eV) indicates that the average bond length is smaller in plane as out of the plane of the film (Natoli's rule - eq. (2)). We must emphasize here that as the va-

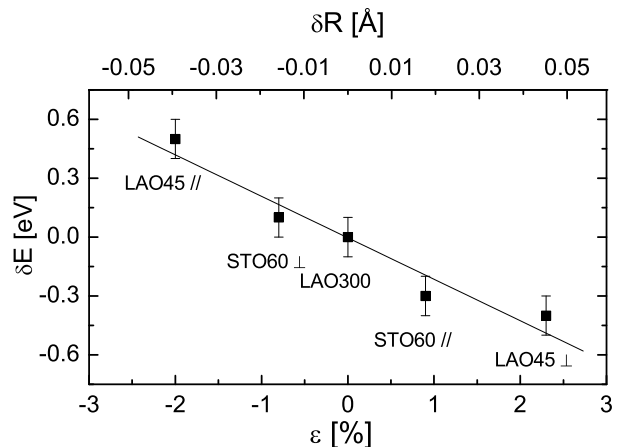


Figure 2: Energy shift at the Mn K-edge relative to the relaxed film, plotted against the strain induced by the substrate. At the top scale, the strain is associated to the local  $Mn-O$  bond lengths.

lence state remain unaltered, all energy shift effects discussed in this paper are related to bond length changes.

We observe that the amplitude of the shift for the LAO45 film is about twice that for the STO60 one, and of the same order as the ratio of the long range strain factor among these films. These results are summarized in the figure 2. The strain on the cell parameters is directly related to average octahedral modifications and suggests a model of tetragonal distortion at the atomic scale. Considering a cluster centered in the manganese, a model structure is built by transforming the coordinates  $(x,y,z)$  of a given atom to  $(x + \epsilon_{\parallel}x, y + \epsilon_{\parallel}y, z + \epsilon_{\perp}z)$ . The angle  $\phi$  is not modified. The length of the  $Mn-O$  bond in the plane and out of the plane of the films are proportional to the corresponding cell parameters and directly derived from the strain factor :  $R_{\parallel} = R_0(1 + \epsilon_{\parallel})$  and  $R_{\perp} = R_0(1 + \epsilon_{\perp})$ .

This model can be confronted with the experimental data using the Natoli's rule (see section II)<sup>23</sup>:  $(E_r - E_b)R^2 = K$ . The resonance considered here is the B resonance corresponding to  $1s \rightarrow 4p$  antibonding  $\sigma^*$  transition. The energy  $E_r$  is then the energy of maximum at the edge. For small changes in the ligand distance  $\delta R = R - R_0$ , resulting in small energy shifts  $\delta E = E_r - E_{r0}$ , with respect to the reference energy  $E_{r0}$ , a linear relationship is obtained by differentiation:  $\delta E = -2 \frac{\delta R}{R_0} (E_{r0} - E_b)$ . In the following the relaxed film LAO300 is taken as reference ( $E_{r0} = 6558.0eV$ ,  $R_0 = 1.948$ ). The experimental energy shift related to the position of main resonance  $\delta E$  can be plotted as a function the variation of distance with respect to the distance  $R_0$ , as introduced by the top scale in figure 2. The relation is linear, in accordance with the Natoli's rule, giving for  $\Delta E_{rb} = E_{r0} - E_b \approx 10.5eV$ .

An additional remark should be made on the comparison of the XANES spectra in strained and relaxed films: the main slope at the absorption edge is larger for the strained films than for the relaxed one, and the derivative (fig. 3) reveals the presence of two contributions (peaks marked by vertical arrows). This result will be discussed in the next section, along with the EXAFS results.



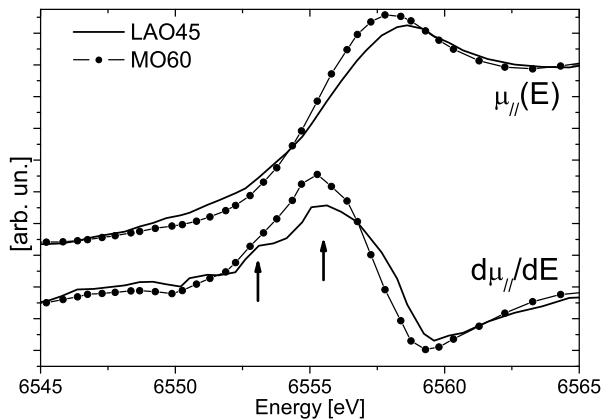


Figure 3: XANES spectra and its derivative for in-plane measurements on LAO45 and MO60 films. The vertical arrows indicate contributions likely coming from two different distances.

The modifications of the main line are not straightforward interpreted by qualitative considerations and we resort to *ab initio* simulations. The clusters used in calculations are build from the structure and cell parameters of  $La_{0.7}Sr_{0.3}MnO_3$  regular octahedron  $MnO_6$  in the symmetric  $D_{3d}^6$  group, and considering only  $La$  in the  $A$  site. Identical calculations were performed with several random combinations of  $Sr$  and  $La$  on this site. These different calculations lead to similar spectra. 21 atoms clusters calculations (central  $Mn$ , 6  $O$  in the coordination shell, 8 ( $La, Sr$ ) atoms and the third shell of 6  $Mn$  atoms) give a good agreement with main features of the experimental spectra, relevant for the present study. As a matter of fact the main features discussed here are determined by the coordination polyhedron. Thence for the simulations of the strained structures only the coordination polyhedra were distorted, and the  $A$  atoms and the  $Mn$  shell are kept in the positions of the relaxed structure, using local order parameters scaling with the crystallographic cell parameters of the films. The 21-atom spectra correspond to a radius  $R_c = 4$  (all calculations use  $RFMS = 4$  and  $RSCF = 4$ ).

The simulations were done using two models for  $MnO_6$ : keeping the  $O_h$  symmetry for  $MnO_6$  or considering a tetragonal distortion. As expected for this isotropic case,  $\mu_{||}$  and  $\mu_{\perp}$  XANES spectra are identical. We also observe that in simulated spectra keeping the  $O_h$  symmetry for  $MnO_6$  the shape of the of the B feature is almost unaltered. Thence a remotion of the octahedra symmetry is necessary to account for the alterations in the XANES spectra of the strained films. The calculations shown in figure 4 were performed for clusters with tetragonal distortion of the  $MnO_6$  “octahedra”. The calculated structures reproduce well the main features of the experimental results. They account as well for the energy shift, in amplitude and direction, as for the relative reduction of the amplitude of the main feature close to the edge, among the two orientations for each film (fig. 1).

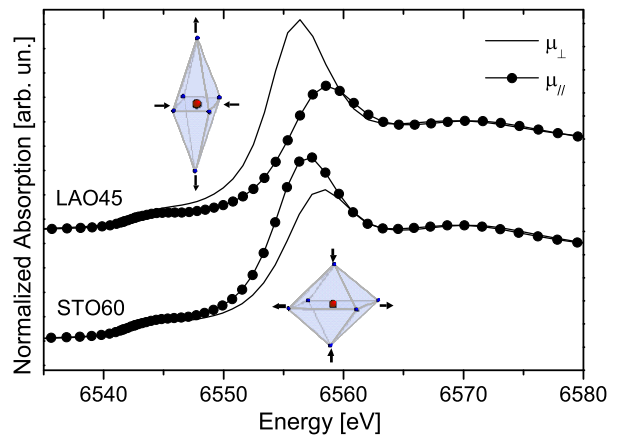


Figure 4: Simulated XANES spectra for the  $\mu_{\perp}$  and  $\mu_{||}$  contribution of the supposed LAO45 and STO60 films structures.

## B. $Mn$ -K EXAFS

As EXAFS signal cannot be collected for LAO45, our study is limited to the STO60 sample. A complete EXAFS characterization of the octahedral deformation would require a measure of the  $Mn - O$  out of plane distance from the  $\mu_{\perp}$ -EXAFS in this sample. As we mentioned in the section II for  $\mu_{\perp}$  measurements the presence of a large number of Bragg peaks associated to a lower flux prevents from the collection of data with proper quality for this analysis. EXAFS signal for  $La_{0.7}Sr_{0.3}MnO_3$  bulk and  $\mu_{||}$  in strained and relaxed films, are shown in figure 5. The extraction of this signal is a critical point when one intends to compare data collected with non-equivalent and relatively low signal over noise ratio. To certify the results we resort to several codes<sup>37,38,39,40</sup> making use of different extraction procedures based on spline or polynomial fits of the atomic background or/and Fourier transform filtering. The tail of the  $La L_1$  XAS spectra ( $E_0 = 6267eV$ ) is largely removed by the signal extraction. It contributes weakly to low frequency component in the EXAFS spectra of the bulk  $La_{0.7}Sr_{0.3}MnO_3$ . Small departure from the bulk-like correction in the films have been neglected. The extension of the EXAFS spectra is limited in the films limiting the  $r$ -space resolution of the study through the relation  $\delta r \cdot \delta k \approx \pi/2$ . However, a discussion of the local distortion in  $La_{0.7}Sr_{0.3}MnO_3$  bulk is out of the scope of this paper. The information we seek here is related to small shifts with respect to a relaxed bulk-like situation, whose spectra are then taken as reference.

The Fourier transform of the EXAFS signal of  $La_{0.7}Sr_{0.3}MnO_3$  bulk is given in the figure 6. The first main peak corresponds to the oxygen coordination shell. In our low resolution data this shell can be properly fitted using calculated amplitude and phases relative of the Mn-O pair on the basis of the crystallographic structure, by assuming one Mn-O distance. According to our comparative approach, we extracted from the signal of this coordination shell, amplitude and phases relative to the Mn-O pairs, that will be later used to refine the data of the films. At higher distance in the

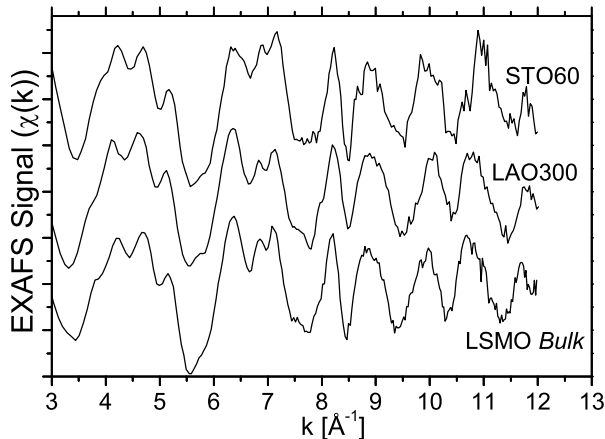


Figure 5: Mn K-edge EXAFS measurements of the films and bulk  $La_{0.7}Sr_{0.3}MnO_3$ .

FT are shown the peaks corresponding to larger effective distances, including the A site neighbours and nearest-Mn single scattering (SS) contributions, as well as the multiple scattering (MS) contributions. In manganite compounds all these contributions must be taken into account together. In the present study we resort to *ab initio* simulations on the basis of the crystallographic structure to evaluate how far the analysis of the Mn next nearest neighbours can be simplified. Due to the high symmetry of atomic distribution around Mn atoms, the contribution of this shell is included in the relatively sharp FT peak at around 3.5 Å. The simulations reveal that so far the low k part ( $k \leq 4.5 \text{ \AA}^{-1}$ ) of the signal and the peak sides and are not included (back Fourier Transform reduced to 3.3-4 Å), the MS is dominated by the contribution the almost collinear of 4-fold paths involving Mn nearest neighbours and their common oxygen. We observe that this path is closely related to the Mn-Mn SS path, because Mn-Mn is one of its legs. The two other legs are Mn-O legs with a focusing angle close to 180, resulting to an effective length of the path very close to Mn-Mn distance. The length variation of the SS and MS dominant paths are then closely related. A variation in the Mn-Mn bond lengths will result, in a good approximation, to an identical variation in the effective length of the MS path. A new MS path can be parameterized constraining its parameters to be the same as those of the SS path. It was verified that a fitting procedure taking into account the two contributions with the same fitting parameters gives a satisfactory sensitivity to a variation of the Mn-Mn distance. Our fits have then been performed in this simple way, using both SS and MS paths, but without adding new variables to the fit, in compatibility with the limited number of independent points.

The signal of first peak of the Fourier transform in relaxed and strain films was back-transformed over the  $R$ -range 0.9 to 2.04 Å for the fitting procedure. We used relative phase and amplitude data obtained by two ways: extracting from experimental data for bulk material and from *ab initio* simu-

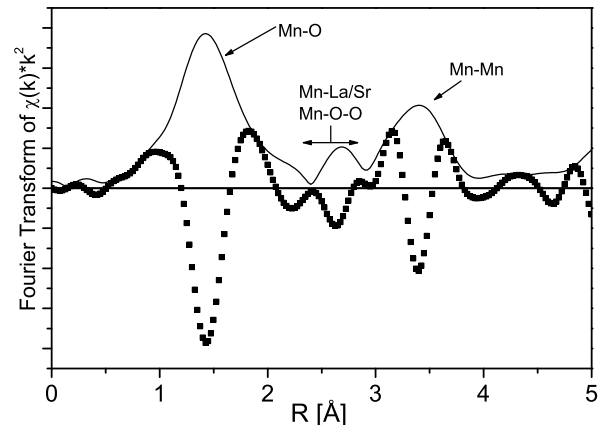


Figure 6: Fourier transform of the EXAFS signal for the tensile film (STO60). The FT modulus (solid line) and the FT imaginary part (points) are shown.

Table II: EXAFS results, for relaxed film (MgO) and under in-plane expansion (STO). Considering only the in-plane contribution.

	Coordination shell ( $Mn-O$ )			
	N	R (Å)	$\sigma^2 \cdot 10^4 (\text{Å}^2)$	$\Delta E_0$ (eV)
STO60	$1.3 \pm 0.5$	$1.94 \pm 0.02$	$17 \pm 5$	$-1.4 \pm 0.2$
	$2.7 \pm 0.5$	$2.05 \pm 0.02$	$17 \pm 5$	$-1.4 \pm 0.2$
MO60	4(fixed)	$1.95 \pm 0.01$	$25 \pm 5$	$-1.4 \pm 0.2$
	$Mn$ next neighboring shell ( $Mn-Mn$ )			
	N	R(Å)	$\sigma^2 \cdot 10^4 (\text{Å}^2)$	$\Delta E_0$ (eV)
STO60	$7 \pm 1$	$3.890 \pm 0.005$	$25 \pm 5$	$0.4 \pm 0.2$
MO60	$6 \pm 1$	$3.875 \pm 0.005$	$13 \pm 5$	$0.4 \pm 0.2$

lations. Identical results are obtained in the two cases. In the relaxed film MO60 (or LA300) a single shell fit with  $Mn-O$  bond of  $(1.95 \pm 0.02)$  accounts for the experimental data. In the strained film STO60, we obtained for the bond length a larger average value ( $Mn-O$ ) of  $(2.01 \pm 0.02)$ . In this case, we should point out that the achievement of repetitive fits of equivalent quality, needed the introduction of two different  $Mn-O$  bonds at  $(1.94 \pm 0.02)$  and  $(2.05 \pm 0.02)$  respectively (table II). One-shell fits lead to non-repetitive or meaningless results and quality factors worse by at least a factor 4.

The signal of Mn nearest neighbors has been selected by back-Fourier transform in the  $R$ -range 3.3 to 3.95. The low range part ( $< 4.5 \text{ \AA}^{-1}$ ), was dismissed. Procedures using backscattering amplitude and phases obtained from a bulk sample give good fits and the  $Mn-Mn$  distances are determined with small relative uncertainties ( $\sim 0.005 \text{ \AA}^{-1}$ ). The relaxed films the  $Mn-Mn$  distance is found to be 3.875, as it is in the bulk compound. In the tensile STO60 film this distance is 3.89, i.e. increased by about 0.02 in comparison to bulk

compound and the relaxed films (table II).

## V. DISCUSSION

From  $\mu_{||}$ -EXAFS we found an average  $Mn-O$  in-plane distance larger in the strained STO60 film as compared to the relaxed samples. This states for an enlargement of the basal  $MnO_4$  square. Much care should be taken, however, on the interpretation of the numerical values associated to these fits. In  $La_{0.7}Sr_{0.3}MnO_3$  bulk compounds it has been observed that the local structure around Mn atoms can be described as well by a model of regular octahedron or a distorted octahedron with different Mn-O distances, these models cannot be unambiguously distinguished even in a high resolution study<sup>21</sup>. In the present low resolution study the absolute value of the variation in  $Mn-O$  distance between strained and relaxed film ( $0.06 \pm 0.04$ ) has a limited significance, and only express the expansion of this distance, in agreement with the XANES analysis.

The  $\mu_{||}$ -EXAFS analysis of the coordination shell, however, rises another comment. It is well settled that in an EXAFS experiment the k-range available limits the minimum distance separation  $\Delta R$  that can be resolved in the analysis. It is usually considered that  $2\Delta k\Delta R$  should be larger than  $\pi$ . From this criteria distance separation lower than  $0.12\text{\AA}$  cannot be unambiguously evidenced in our study. However we consider that the tendency to obtain two separate sub-shells for the fit of the coordination shell in the constrained film STO60 should be noted. We should stress that our approach is comparative and that, when a two-shell fit is performed with the same conditions in the relaxed samples, the two distances invariably collapse to give one unique value. This indication of the possible coexistence of two distances in the plane has to be related to another experimental evidence obtained from the study of the rising edge in constrained films, where two contributions were observed (fig.3). These observations can lead to two different conclusions. In a first hand the biaxial strain may induce an additional unexpected small additional distortion of the basal plane of the  $MnO_6$  octahedra. This distortion would express a tendency to recover a Jahn-Teller distortion in this plane. On the other hand the observation of two distances can be related to the existence of two domains with different relaxation states, as observed by Qian et al.<sup>17</sup> in  $Nd_{0.5}Sr_{0.5}MnO_3$ . Depth sensitive local probe as X-ray absorption measurements at grazing angle would be necessary to settle this point. No quantitative evaluation of this -clearly very small- splitting can be given and it will be dismissed in the following.

Based on the differential Natoli's rule,  $\delta E = -2\frac{\delta R}{R_0}(E_r - E_b)$ , and on the model of tetragonal distortion for the octahedra reflecting the film strain, we deduce from the slope of the curve in figure 2  $\Delta E_{rb} = (E_r - E_b) = 10.5 \pm 0.1\text{eV}$ . Using the  $Mn-O$  distance of  $1.95\text{\AA}$  of the relaxed films, a constant  $K$  of about  $41\text{eV}\cdot\text{\AA}^2$  is found. This value is close to that obtained for Cu-O bonds in high temperature superconductors<sup>25</sup>. Due to the electronic similarities between these two metallic perovskite systems, the interstitial potentials are expected to be similar. The value of  $\Delta E_{rb}$  fix the position of the bond level

$E_b$  in the XANES spectra. The energy of the resonance B is  $6558\text{eV}$  in the relaxed spectra, so that  $E_b = 6547\text{eV}$ , about  $4\text{eV}$  above the pre-edge structure (A) and close to the onset of the main edge (fig.1). It is worth noting that the actual position of the bond level for Cu-O in high temperature cuprates is also few eV apart from the pre-edge features<sup>25</sup>. The agreement between constant K and the reasonable value for the bonding energy express the validity of the model. We consider that for the coordination shell the values determined by XANES analysis far more precise than those obtained from EXAFS and further discussion is based on these values.

The first important statement deduced from our XANES results is that  $MnO_6$  geometry is directly affected by the strain and cannot then be considered as fully determined by the stoichiometry of the compound. This statement is in agreement with the findings of Qian and coworkers<sup>17</sup> in a quite different system and could then be generalized in manganite films. These findings stress the importance of the distortion of the ligand field around the manganese atoms.

In the bulk LSMO system, the  $MnO_6$  octahedra can be consider as regular. In the thin films the distortion of the  $MnO_6$  octahedra induced by the strain can be expressed by  $\sigma = \sqrt{\frac{1}{3}\sum_i [(Mn-O)_i - \langle Mn-O \rangle]^2}$ , in a similar way that for Jahn-Teller distortion. Using the values deduced from XANES analysis we have  $\sigma = 0.041$  for the LAO45 film, about one third of the Jahn-Teller distortion in  $LaMnO_3$ . The trapping of the  $e_g$  electrons at the  $Mn$  site by such tetragonal "Jahn-Teller like" distortion may largely be responsible for the lowering of the Curie temperature observed in these films. The strain-induced modification in the film magnetic and transport properties should be ascribed to the variations of hybridization between the metal and ligand orbitals and a reduced transfer interaction  $t_{pd}^0$ , reducing the double exchange by localizing the  $e_g$  electron.

The increase of the  $Mn-Mn$  distance is determined by EXAFS analysis with a good accuracy. In the tensile STO60 film this distance is increased by 0.02 in comparison to bulk compound and the relaxed films. This corresponds to a relative variation of 1%, matching the cell parameters and of the order of the increase of the  $Mn-O$  distance, as found by XANES analysis. Consequently the  $\phi$  angle is not -or very weakly- modified. This results are conflicting with those obtained by Miniotas et al.<sup>16</sup> in  $La_xCa_{1-x}MnO_3$  films. In almost equivalent strain conditions, they reported variations of about  $8^\circ$  in the  $\phi$  angle, and no variation in the  $Mn-O$  distance. They consequently conclude that the biaxial strain is accommodated by appropriated modification of the tilt angle. The modification of the  $Mn-O$  distance is unambiguously shown by our XANES data. Due to the accuracy on the distance determination and the large angles involved (around  $165^\circ$ ) we cannot conclude about possible small variations ( $<2-3^\circ$ ) of the tilt angle. A limited variation in the tilt angle  $\phi$  may indeed exist. However we have shown that a model of accommodation at the atomic scale of the strain experienced by the cell, accounts perfectly for the XANES data, so that tilt angle variation is not necessary to this accommodation. Hence we believe that, in spite of the well established theoretical background and experimental evidence of the influence of the tilt

angle on the magnetic properties in bulk manganites, the tilt angle is neither the only nor the main driving factor of the modification of these properties in strained manganite films.

## VI. CONCLUSIONS

We presented here a characterization by an angle-resolved X-ray absorption spectroscopy, of the local scale structural distortion induced by substrate epitaxial strain around manganese atoms in  $La_{0.7}Sr_{0.3}MnO_3$  films. We show that biaxial strain is locally accommodated in the coordination shell, by distortion of the  $MnO_6$  octahedron, without change in the tilt angle. These findings refuse the scenarios where  $MnO_6$  octahedron would be entirely determined by the stoichiometry of

the compound and a tilt in the octahedral linkage would be the only driving parameter in the strain dependence of the transport and magnetic properties of manganites thin films. We believe that changes within the octahedra, with an induced tetragonal “Jahn-Teller like” distortion, should have also a predominant role in the modification of these properties.

## Acknowledgments

The authors would like to thank Dr. J. Mustre de Leon for fruitful discussions. This work is partially supported by LNLS/ABTLuS/MCT and FAPESP (1999/12330-6). NMSN and AYR acknowledges the grants from CAPES and CNPq respectively.

- 
- \* Also at: Instituto de Física Gleb Wataghin, IFGW - UNICAMP, Campinas, SP, Brazil; Electronic address: narcizo@lnls.br
- † Also at: Laboratoire de Minéralogie-Cristallographie de Paris, LMCP -UMR 7590 -CNRS, Paris, France
- <sup>1</sup> S. Jin, T. H. Tiefel, M. McCormack, R. A. Fastnacht, R. Ramesh, and L. H. Chen, *Science* **264**, 413 (1994).
  - <sup>2</sup> A. J. Millis, *Nature* **392**, 147 (1998).
  - <sup>3</sup> Y. Murakami, J. H. Yoo, D. Shindo, T. Atou, and M. Kikuchi, *Nature* **423**, 965 (2003).
  - <sup>4</sup> R. Mahesh, R. Mahendiran, Raychaudhuri, and C. Rao, *J. Solid. State Chem.* **120**, 204 (1999).
  - <sup>5</sup> R. Mahendiran, S. K. Tiwary, A. K. Raychaudhuri, T. V. Ramakrishnan, R. Mahesh, N. Rangavittal, and C. N. R. Rao, *Phys. Rev. B* **53**, 3348 (1996).
  - <sup>6</sup> J. Fontcuberta, B. Martínez, A. Seffar, S. Piñol, J. L. García-Muñoz, and X. Obradors, *Phys. Rev. Lett.* **76**, 1122 (1996).
  - <sup>7</sup> Y. Moritomo, A. Asamitsu, and Y. Tokura, *Phys. Rev. B* **51**, 16491 (1995).
  - <sup>8</sup> W. Prellier, P. Lecoeur, and B. Mercey, *J. Phys.: Condens. Matter* **13**, R915 (2001).
  - <sup>9</sup> A. J. Millis, T. Darling, and A. Migliori, *J. Appl. Phys.* **83**, 1588 (1998).
  - <sup>10</sup> H. Wang, Q. Li, K. Liu, and C. Chien, *Appl. Phys. Lett.* **74**, 2212 (1999).
  - <sup>11</sup> L. Ranno, A. Llobet, R. Tiron, and E. Favre-Nicolin, *Applied Surface Science* **188**, 170 (2002).
  - <sup>12</sup> M. Bibes, S. Valencia, L. Balcells, B. Martínez, J. Fontcuberta, M. Wojcik, S. Nadolski, and E. Jedryka, *Phys. Rev. B* **66**, 134416 (2002).
  - <sup>13</sup> P. G. Radaelli, G. Iannone, M. Marezio, H. Y. Hwang, S.-W. Cheong, J. D. Jorgensen, and D. N. Argyriou, *Phys. Rev. B* **56**, 8265 (1997).
  - <sup>14</sup> W. Prellier, A. M. Haghiri-Gosnet, B. Mercey, P. Lecoeur, M. Hervieu, C. Simon, and B. Raveau, *Appl. Phys. Lett.* **77**, 1023 (2000).
  - <sup>15</sup> D. Cao, F. Bridges, D. C. Worledge, C. H. Booth, and T. Geballe, *Phys. Rev. B* **61**, 11373 (2000).
  - <sup>16</sup> A. Miniotas, A. Vaillonis, E. B. Svedberg, and U. O. Karlsson, *J. Appl. Phys.* **89**, 2134 (2001).
  - <sup>17</sup> Q. Qian, T. A. Tyson, C.-C. Kao, W. Prellier, J. Bai, A. Biswas, and R. L. Greene, *Phys. Rev. B* **63**, 224424 (2001).
  - <sup>18</sup> A. Urushibara, Y. Moritomo, T. Arima, A. Asamitsu, G. Kido, and Y. Tokura, *Phys. Rev. B* **51**, 14103 (1995).
  - <sup>19</sup> X. W. Wu, M. S. Rzchowski, H. S. Wang, and Q. Li, *Phys. Rev. B* **61**, 501 (2000).
  - <sup>20</sup> V. R. Mastelaro, D. P. F. de Souza, and R. A. Mesquita, *X-Ray Spectrometry* **31**, 154 (2002).
  - <sup>21</sup> T. Shibata, B. A. Bunker, and J. F. Mitchell, *Phys. Rev. B* **68**, 024103 (2003).
  - <sup>22</sup> N. M. Souza-Neto, A. Y. Ramos, H. C. N. Tolentino, E. Favre-Nicolin, and L. Ranno, *Appl. Phys. Lett.* **83**, 3587 (2003).
  - <sup>23</sup> C. Natoli, in *EXAFS and Near edge structure III*, edited by B. H. K.O Hodgson and J. Penner-Hahn (Springer-Verlag, 1984), pp. 38–42, Springer Proceedings in Physics 2.
  - <sup>24</sup> C. Brouder, *J. Phys. Condens. Matter* **2**, 701 (1990).
  - <sup>25</sup> H. Tolentino, F. Baudelet, A. Fontaine, T. Gourieux, G. Krill, J. Y. Henry, and J. Rossat-Mignod, *Physica C* **192**, 115 (1992).
  - <sup>26</sup> E. Gaudry, A. Kiratisin, P. Sainctavit, C. Brouder, F. Mauri, A. Ramos, A. Rogalev, and J. Goulon, *Phys. Rev. B* **67**, 094108 (2003).
  - <sup>27</sup> H. Magnan, D. Chandesris, B. Villette, O. Heckmann, and J. Lecante, *Phys. Rev. Lett* **67**, 859 (1991).
  - <sup>28</sup> S. Pizzini, F. Baudelet, D. Chandesris, A. Fontaine, H. Magnan, J. M. George, F. Petroff, A. Barthelemy, A. Fert, R. Loloee, et al., *Phys. Rev. B* **46**, 1253 (1992).
  - <sup>29</sup> D. C. Koningsberger and R. Prins, eds., *X-Ray Absorption: Principles, Applications, Techniques of EXAFS, SEXAFS and XANES*, vol. 92 of *Chemical Analysis* (John Wiley and Sons, 1988).
  - <sup>30</sup> A. L. Ankudinov, B. Ravel, J. J. Rehr, and S. D. Conradson, *Phys. Rev. B* **58**, 7565 (1998).
  - <sup>31</sup> E. Favre-Nicolin, Ph.D. thesis, Université Joseph Fourier - Grenoble I, France (2003).
  - <sup>32</sup> H. C. N. Tolentino, A. Y. Ramos, M. C. M. Alves, R. A. Barrea, E. Tamura, J. C. Cezar, and N. Watanabe, *J. Synchrotron Rad.* **8**, 1040 (2001).
  - <sup>33</sup> H. C. N. Tolentino, J. C. Cezar, N. M. Souza-Neto, and A. Y. Ramos, *J. Synchrotron Rad.*, submitted (2004).
  - <sup>34</sup> T. A. Tyson, J. MustredeLeon, S. D. Conradson, A. R. Bishop, J. J. Neumeier, H. Röder, and J. Zang, *Phys. Rev. B* **53**, 13985 (1996).
  - <sup>35</sup> M. Croft, D. Sills, M. Greenblatt, C. Lee, S.-W. Cheong, K. V. Ramanujachary, and D. Tran, *Phys. Rev. B* **55**, 8726 (1997).
  - <sup>36</sup> Q. Qian, T. A. Tyson, C.-C. Kao, M. Croft, S.-W. Cheong, G. Popov, and M. Greenblatt, *Phys. Rev. B* **64**, 024430 (2001).
  - <sup>37</sup> K. V. Klementev, *J. Phys. D: Applied Physics* **34**, 209 (2001).
  - <sup>38</sup> A. Michalowics, Ph.D. thesis, Université du Val de Marne, France



(1990).  
<sup>39</sup> B. Ravel, E. Cockayne, M. Newville, and K. M. Rabe, Phys. Rev. B. **60**, 14632 (1999).

<sup>40</sup> T. Ressler, J. Phys. IV **7**, C2 (1997).